Available online at www.sciencedirect.com
ScienceDirect
Polyhedron 26 (2007) 2320–2324
POLYHEDRON
www.elsevier.com/locate/poly

^{55}Mn nuclear spin relaxation in the truly axial single-molecule magnet Mn_{12}-*t*-butylacetate thermally-activated down to 400 mK

A.G. Harter [a], C. Lampropoulos [b], M. Murugesu [b], P. Kuhns [a], A. Reyes [a], G. Christou [b], N.S. Dalal [a,*]

[a] *Department of Chemistry and Biochemistry and National High Magnetic Field Laboratory, Florida State University, Tallahassee, FL 32306, USA*
[b] *Department of Chemistry, University of Florida, Gainesville, FL 32611, USA*

Received 21 September 2006; accepted 19 November 2006
Available online 1 December 2006

Abstract

We report on the measurements of the spin–lattice relaxation time, T_1, of $Mn_{12}O_{12}(O_2CCH_2Bu^t)_{16}(CH_3OH)_4 \cdot CH_3OH$, a truly axial symmetry Mn_{12} single-molecule magnet (SMM), with the view to examining the role of point symmetry and lattice-solvate molecules in this Mn_{12} SMM. The measurements were made over 0.390–1.8 K, on freshly prepared single crystals which afforded much higher spectral resolution than magnetically aligned powder. The measured T_1 is found to be thermally activated, and follows either a T^2 or exponential behavior over 0.390–0.7 K, in contrast to the temperature-independent behavior for Mn_{12}-acetate, where Jahn–Teller isomers are thought to be the origin of the temperature-independent nuclear relaxation mechanism.

Keywords: Single-molecule magnets; SMM; NMR; T_1; He-3; ^{55}Mn

1. Introduction

Single-molecule magnets (SMMs) have been an active area of research for over a decade now [1]. Sustained interest in these molecules is a result of the newly discovered quantum tunneling of magnetization (QTM) phenomena inherent in these systems, which implicates the possibilities associated with quantum computing and magnetic memory storage at the molecular dimension [2,3]. The first SMM, $[Mn_{12}O_{12}(CH_3COO)_{16}(H_2O)_4] \cdot 2CH_3COOH \cdot 4H_2O$ (Mn_{12}-Ac) [4], is by far the most investigated system [5]. Recently, however, Mn_{12}-Ac has been shown to be a heterogeneous compound, in that there are at least four different variants of the molecule, owing to the different numbers of CH_3COOH solvate molecules surrounding the Mn_{12} core, as recognized first by Cornia et al. [6]. Originally, it was thought that these distortions provided a mechanism by which QTM could be enhanced, however, this has been contradicted by the more recent synthesis of highly homogenous SMMs, which are derivatives of Mn_{12}-Ac and exhibit similar behavior [7]. Specifically, $[Mn_{12}O_{12}(O_2CCH_2Br)_{16}(H_2O)_4] \cdot 4CH_2Cl_2$ (Mn_{12}-BrAc), and $[Mn_{12}O_{12}(O_2CCH_2Bu^t)_{16}(MeOH)_4] \cdot MeO\ H$ (Mn_{12}-*t*-Bu), the latter shown in Fig. 1 [8]. Two recent reports on Mn_{12}-BrAc have displayed the possibilities of chemically altering these materials by ligand substitution, changing the physical properties and allowing a detailed comparison with known compounds [9,10]. On the other hand, very little information has been reported on Mn_{12}-*t*-Bu, prompting the current study. Comparison within a family of SMMs can provide information that would otherwise be hard to determine experimentally, such as the role that spin diffusion or loss of local symmetry plays as we increase the size of the ligands, keeping the core of the molecule the same.

Mn_{12}-*t*-Bu, like Mn_{12}-Ac, is composed of four Mn^{4+} ($S = 3/2$) ions and eight Mn^{3+} ($S = 2$) ions [8]. The

* Corresponding author.
E-mail address: dalal@chemmail.chem.fsu.edu (N.S. Dalal).

0277-5387/$ - see front matter © 2006 Elsevier Ltd. All rights reserved.
doi:10.1016/j.poly.2006.11.039

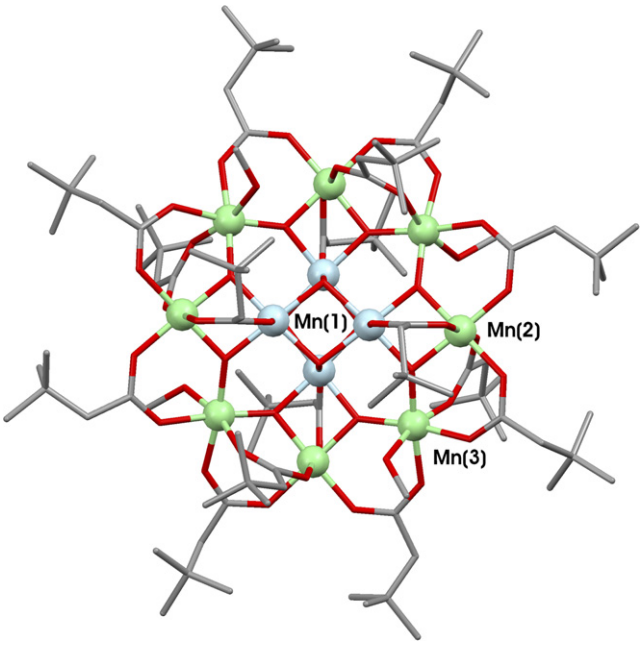

Fig. 1. Mn_{12}-*t*-Bu crystal structure.

Mn^{3+} ions are ferromagnetically coupled to each other and form a ring around the cubane-like (Mn_4O_4) structure of the Mn^{4+} ions, which are also ferromagnetically coupled. The interaction between the Mn^{3+} and Mn^{4+} ions, however, is antiferromagnetic, giving a total spin, $S_T = 10$. The electronic Hamiltonian representing this system is then given (assuming a giant spin model) as

$$\mathscr{H} = \mu_B H \cdot g \cdot S + DS_z^2 + B_4^0 O_4^0 + B_4^4 O_4^4 + \mathscr{H}',$$

where the first term represents the Zeeman interaction, and for our purposes is zero (because we apply no external field). D is the axially anisotropic zero-field splitting parameter and is followed by higher order crystal field terms; the last term representing rather small perturbations. For the case of Mn_{12}-*t*-Bu: $D = -0.665$ K, $B_4^0 = -0.036$ mK, and $B_4^4 = -0.062$ mK, as established by EPR [11]. The negative axial anisotropy makes the $m_S = \pm 10$ levels the ground state and can be thought of as a type of double potential well. Because our experiments are performed at 3 K and below, our only excitations occur in the ground state of the system, which is where we would like to probe the QTM mechanism. The nuclei at these temperatures are relaxed through the coupling of the electrons to the phonons, thus, nuclear relaxation measurements give insight into the dynamics of the electronic system, which is why this technique has been chosen. To this end we have measured the spectrum and spin–lattice relaxation (T_1) of Mn_{12}-*t*-Bu and show that, in zero external field, the electron relaxation from 700 mK to 400 mK does not occur dominantly through a tunneling mechanism.

2. Synthesis and crystal growth

Mn_{12}-*t*-Bu is synthesized by a carboxylate substitution of Mn_{12}-Ac followed by re-crystallization with CH_3OH/Et_2O, as described elsewhere [8b]. The crystals were dark with a brick shape and had dimensions of 1 mm × 1 mm × 2 mm.

3. NMR experimental details

^{55}Mn NMR measurements were made using a locally developed MAGRes2000 Integrated Wideband NMR spectrometer with quadruture detection and a home built high frequency probe [12,13]. For the measurement of the spectrum, samples were prepared by removing the crystal from its mother liquor and immediately covering in 5-min epoxy to prevent crystal fractures after thermal cycling. Immediately after the epoxy was set, the sample was mounted into the coil and cooled in a dewar of liquid Helium. The spectrum was acquired at 1.45 K, below the blocking temperature, T_B, of ~3 K because of fast T_2 times above this temperature. A Hahn echo pulse sequence was used while the frequency was scanned from 220 MHz to 400 MHz, usually taking 0.25 MHz steps. Frequency scans were necessary because of the large peak widths (~5–20 MHz). Pulse lengths were of the order of 500 ns.

Preparation of the sample for He-3 measurements consists of surrounding the crystal with N-grease before placing into a coil. He-3 experiments were performed in a Janis cryostat. The system is capable of maintaining ~380 mK for 12 h with the heat load from the NMR probe and pulses. After that time, the He-3 is re-condensed. T_1 measurements were conducted on the Mn^{4+}, Mn(1) peak, down to 390 mK. In order to saturate any quadrupole split peaks, we apply a frequency hopping comb pulse, discussed in a previous publication [9]. This comb pulse is repeated up to 20 times to ensure the spins are perturbed from equilibrium. Evidence for this is seen in the good fits of the relaxation data to a single exponential function. Any deviation from exponential is due to the fact that we are unable to achieve full saturation. The T_1 data are fit to the following exponential, as reported earlier [9]: $M(t) = (M_\infty - M_0)[1 - \exp(-t/T_1)] + M_0$, where $M(t)$ is the time dependent nuclear magnetization, M_∞ is the equilibrium magnetization, t is the time between the saturation sequence and the observation spin-echo, M_0 is the remnant magnetization immediately following the saturation comb, and T_1 is the longitudinal (spin–lattice) relaxation time.

4. Results

As shown in Fig. 2, the ^{55}Mn NMR spectrum of Mn_{12}-*t*-Bu exhibits three sets of peaks, the two Mn^{3+} ion environments and the Mn^{4+} ion environment, essentially similar to those for Mn_{12}-Ac and Mn_{12}-BrAc [9,10,14,15]. Peaks are assigned by considering the number of unpaired electrons at each Mn site, along with any Jahn–Teller distortion

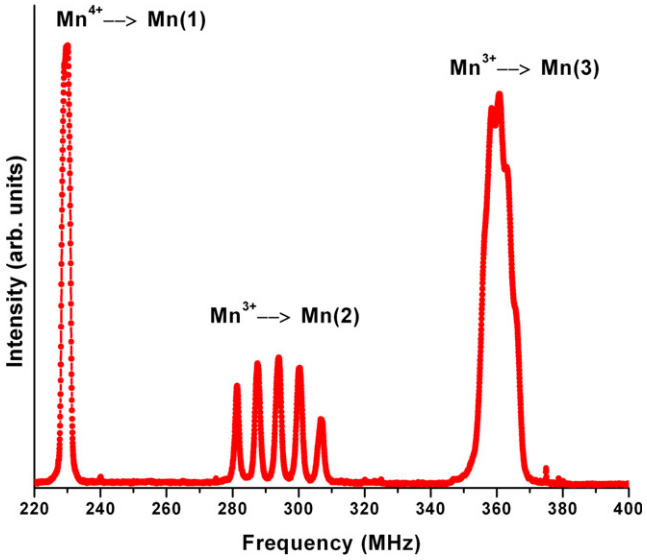

Fig. 2. Single crystal ^{55}Mn NMR spectrum of Mn_{12}-*t*-Bu.

[14]. Because the Mn^{4+} ions have one less electron than the Mn^{3+} ions, it is expected that the Mn^{4+} Fermi Contact hyperfine field will be smaller, thus resulting in a lower resonance frequency. Also, because the Mn^{4+} ion is in an environment of electron distribution which is close to cubic, we do not expect there to be a large quadrupole splitting. The Mn(1) peak at 230.1 MHz (21.91 T) can then be assigned to the Mn^{4+} ions. The full width at half maximum (FWHM) is 2.8 MHz, which is broad when compared against the Mn(2) peaks FWHM of 1.9 MHz. A closer examination of the Mn(1) peak shows structure at the apex, indicating the presence of quadrupolar interactions, which would result in a broadened peak. Isomers could also increase the peak width, similar to that seen in Mn_{12}-Ac [10], however, there is no clear evidence for isomers after examination of the Mn(2) peak. If in fact the Mn(1) peak is split by quadrupole effects, then the Mn^{4+} ions no longer exist in a cubic environment.

The Mn(2) and Mn(3) peaks are assigned by considering their X-ray structure (Fig. 1). The angle the local Jahn–Teller axis makes with the molecular *c*-axis governs the strength of the quadrupole and dipolar interaction. The smaller the angle, the larger the quadrupole splitting and dipolar contribution will be. Because the dipolar hyperfine term is opposite in sign to the Fermi contact term (the main contributor to the hyperfine field), a larger dipole interaction will result in a smaller effective hyperfine field (lower resonant frequency) felt at the nuclear site [14].

The Mn(2) peak, with the largest quadrupole frequency and lower resonant frequency, can then be assigned to the four Mn^{3+} ions which are slightly tilted away from the *c*-axis with an angle of ~13.7°. The central peak for the quadrupolar split resonance is located at 294.0 MHz, has an internal field of 28.00 T, and a FWHM of 1.9 MHz. The separation between each resonance, $\Delta\nu_Q \sim 6.4$ MHz, results in $e^2qQ \sim 46.6$ MHz; with the quadrupole energies being obtained from the following equation:

$$E_m = -\gamma_n \hbar H_0 m_n + \frac{e^2qQ}{4I(2I-1)}\left(\frac{3\cos^2\theta - 1}{2}\right)[3m_n^2 - I(I+1)]$$

The first term is a result of the effective hyperfine splitting and the second term is the quadrupole perturbation. eQ is the electric quadrupole moment, eq is the gradient of the electric field along the *z*-axis, and θ is the angle the Jahn–Teller axis makes with the crystallographic *c*-axis. Taking the energy difference between two neighboring m_n levels allows the calculation of e^2qQ.

The Mn(3) peak has a central frequency of 360.8 MHz resulting in an internal field of 34.36 T. It is also split by quadrupole interactions as a result of its 36.6° tilt of the local Jahn–Teller axis with respect to the molecular *c*-axis. Because of the larger angle, the quadrupolar and dipole terms are smaller, making assignment of this peak straight forward. For Mn(3), $e^2qQ \sim 36.1$ MHz is calculated taking the separation between each resonance, $\Delta\nu_Q \sim 2.5$ MHz.

While the bulkier ligands provide a greater separation among Mn_{12} molecules, diminishing intercluster dipolar effects, they also provide a small distortion in the local electron symmetry, evidenced by the quadrupole splitting of the Mn(1) peak. Although isomers do not appear to be present in this system, the loss of local symmetry gives Mn_{12}-BrAc the advantage of a being the model system for SMMs. However, in terms of sample stability, it seems that Mn_{12}-*t*-Bu is superior, as no asymmetry is seen in any of the resonance signals. Previous studies on Mn_{12}-BrAc do show asymmetry in the first and third peaks and are thought to be a result of sample degradation [10,11]. Even the freshest crystals of Mn_{12}-BrAc exhibit this behavior. Thus, the bulkier ligands in Mn_{12}-*t*-Bu seem to protect the core molecule from the effects that interstitial solvent loss may have on smaller systems.

T_1 measurements of the Mn(1) peak show very similar behavior to the two previously studied Mn_{12} compounds (Mn_{12}-Ac and Mn_{12}-BrAc) in the high temperature limit (Fig. 3) and are fit in a similar manner to that previously reported [9,16] (solid line in Fig. 3) using,

$$T_1^{-1} \approx C\exp(-\Delta E/T), \text{ with } C \approx \frac{\gamma_N^2\langle h_\perp^2\rangle}{\omega_N^2\tau_0},$$

resulting in a pre-exponential factor of $C \sim 1.64 \times 10^5\ s^{-1}$ and a activation energy of $\Delta E = 13.1$ K, corresponding well with the separation between the $m_S = \pm 10$ and $m_S = \pm 9$ states.

Upon reducing the temperature below 0.8 K, we see a dramatic increase in the spin–lattice relaxation time. In fact, at 400 mK $T_1 \sim 1000$ s, roughly three times as long as Mn_{12}-BrAc and an order of magnitude longer than Mn_{12}-Ac, partly a result of the bulkier ligands. The data at these temperatures follows either a T^2 or exponential type of dependence (Fig. 4). It is obvious that QTM is not the dominant relaxation mechanism in this temperature range as this would produce a temperature-independent relaxation region.

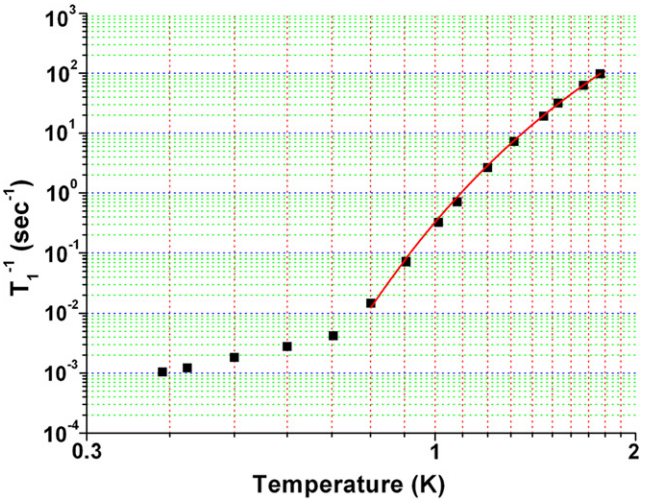

Fig. 3. Inverse T_1 of the Mn(1) peak of Mn_{12}-*t*-Bu single crystal.

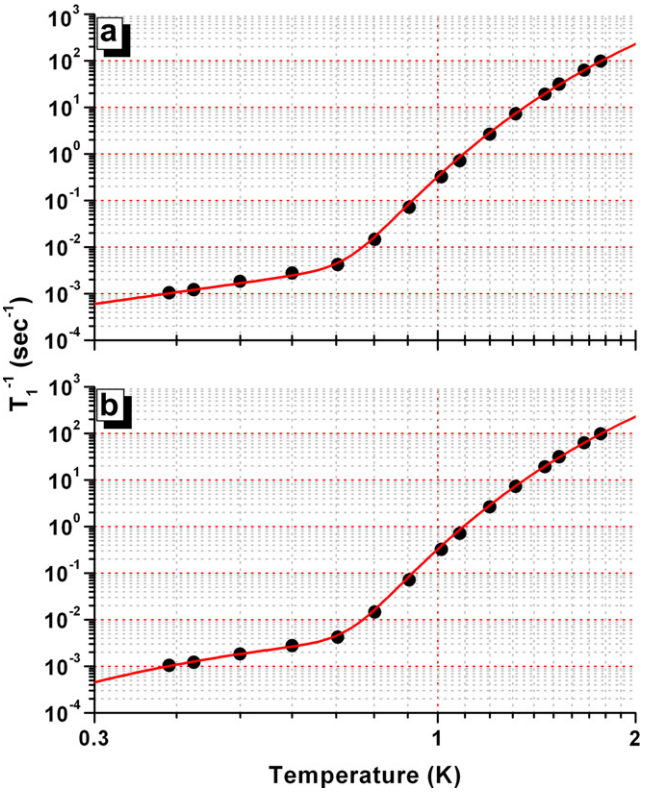

Fig. 4. Inverse T_1 of the Mn(1) peak of Mn_{12}-*t*-Bu single crystal with high and low temperature fit: (a) low temperature fit is a T^2 dependence and (b) low temperature fit is exponential in temperature.

5. Discussion and conclusion

This study again shows that ^{55}Mn NMR using single crystals consistently provides higher resolution data than crushed aligned powders. Of the high symmetry molecules, Mn_{12}-BrAc and Mn_{12}-*t*-Bu, both offer impressive potential for investigation as new model SMM compounds. While Mn_{12}-*t*-Bu shows evidence for the loss of cubic symmetry at the Mn^{4+} site, the sample shows no asymmetry in its peaks, in contrast to Mn_{12}-Ac and Mn_{12}-BrAc, thus attesting to be a more solvate-tough lattice.

The bulky ligands of the Mn_{12}-*t*-Bu also reduce intercluster interactions, greatly increasing the length of T_1 for this compound in the low temperature limit ($T_1 \sim 1000$ s at 400 mK). The data also clearly show a temperature dependence over the entire range studied, indicating that tunneling is not the dominant mechanism by which the nuclei are relaxed. The low temperature (below 0.7 K) thermally-activated nuclear T_1 observed for Mn_{12}-*t*-Bu here, and earlier for Mn_{12}-BrAc [9] is in sharp contrast to the temperature-independent behavior reported for Mn_{12}-Ac by Morello et al. [16], and ascribed to the relaxation caused by the so-called 'fast relaxing' isomers (estimated to be present in 5–8% concentration in crystals of Mn_{12}-Ac). These fast-relaxing isomers have a much lower anisotropy barrier, and lower symmetry (Jahn–Teller axes deviating from their easy axes), and they exhibit tunneling in zero field. On the other hand, the standard Mn_{12}-Ac molecules have their Jahn–Teller axes parallel to the easy (*c*-axis), including the solvent isomers [1,17]. Since no such fast-relaxing species are present in Mn_{12}-*t*-Bu, one may surmise that this compound should show a different nuclear relaxation behavior than Mn_{12}-Ac. Nevertheless, both Mn_{12}-BrAc and Mn_{12}-*t*-Bu show a definitive change in the slope of their nuclear T_1 below about 0.8 K.

Above 0.8 K, the T_1 follows the model of nuclear relaxation via electronic spin fluctuations between the $M_S = \pm 10$ and $M_S = \pm 9$ states. Clearly, once nuclear relaxation by spin fluctuations freezes out below ~0.8 K, some other relaxation process takes over. The details of this new process remain unclear at this point, although the exponential fit to the data between 0.39 K and 0.70 K reveals that there might be a lower temperature barrier of about 1.1 K. Further studies using Mn_{12}-Ac, and at temperatures lower than 0.39 K should prove helpful to understand this process, and are being contemplated.

Acknowledgement

This work was supported by the NSF-DMR Grant # DMR 0506946.

References

[1] (a) D. Gatteschi, R. Sessoli, J. Villain, Molecular Nanomagnets, Oxford University Press, 2006;
(b) G. Christou, Polyhedron 24 (2005) 2065;
(c) D. Gatteschi, R. Sessoli, J. Mag. Mag. Mater. 272-276 (2004) 1030;
(d) D. Gatteschi, R. Sessoli, Angew. Chem., Int. Ed. 42 (2003) 268.
[2] M.N. Leunberger, D. Loss, Nature (London) 410 (2001) 789.
[3] S. Hill, R.S. Edwards, N. Aliagga-Alcade, G. Christou, Science 302 (2003) 1015.
[4] T. Lis, Acta Crystallogr. B36 (1980) 2042.
[5] (a) J.R. Friedman, M.P. Sarachik, J. Tejada, R. Ziolo, Phys. Rev. Lett. 76 (1996) 3830;

(b) L. Thomas, P. Lionti, R. Ballou, D. Gatteschi, R. Sessoli, B. Barbara, Nature (London) 383 (1996) 145;
(c) A.L. Barra, D. Gatteschi, R. Sessoli, Phys. Rev. B 56 (1997) 8192;
(d) M. Hennion, L. Pardi, I. Mirebeau, E. Suard, R. Sessoli, A. Canneschi, Phys. Rev. B 56 (1997) 8819;
(e) J.A.A.J. Perenboom, J.S. Brooks, S. Hill, T. Hathaway, N.S. Dalal, Phys. Rev. B 58 (1998) 330;
(f) S. Hill, J.A.A.J. Perenboom, N.S. Dalal, T. Hathaway, T. Stalcup, J.S. Brooks, Phys. Rev. Lett. 80 (1998) 2453;
(g) Z. Kutnjak, C. Filipic, A. Levstik, R.M. Achey, N.S. Dalal, Phys. Rev. B 59 (1999) 11147;
(h) A.B. Sushkov, B.R. Jones, J.L. Musfeldt, Y.J. Wang, R.M. Achey, N.S. Dalal, Phys. Rev. B 63 (2001) 214408;
(i) W. Wernsdorfer, M. Soler, G. Christou, D.N. Hendrickson, J. Appl. Phys. 91 (2002) 7164;
(j) S. Hill, S. Maccagnano, K. Park, R.M. Achey, J.M. North, N.S. Dalal, Phys. Rev. B 65 (2002) 224410;
(k) K. Park, M.A. Novotny, N.S. Dalal, S. Hill, P.A. Rikvold, Phys. Rev. B 65 (2002) 014426;
(l) Y. Furukawa, K. Watanabe, K. Kumagai, F. Borsa, T. Sasaki, N. Kobayashi, D. Gatteschi, Phys. Rev. B 67 (2003) 064426;
(m) S. Hill, R.S. Edwards, S.I. Jones, N.S. Dalal, J.M. North, Phys. Rev. Lett. 90 (2003) 217204;
(n) E. del Barco, A.D. Kent, E.M. Rumberger, D.N. Hendrickson, G. Christou, Phys. Rev. Lett. 91 (2003) 047203;
(o) S. Takahashi, R.S. Edwards, J.M. North, S. Hill, N.S. Dalal, Phys. Rev. B 70 (2004) 094429.

[6] A. Cornia, R. Sessoli, L. Sorace, D. Gatteschi, A.L. Barra, C. Daiguebonne, Phys. Rev. Lett. 89 (2002) 257201.

[7] (a) K. Petukhov, S. Hill, N.E. Chakov, K.A. Abboud, G. Christou, Phys. Rev. B 70 (2004) 054426;
(b) W. Wensdorfer, M. Murugesu, G. Christou, Phys. Rev. Lett. 96 (2006) 057208.

[8] (a) J. An, Z.-D. Chen, X.-X. Zhang, H.G. Raubenheimer, C. Esterhuysen, S. Gao, G.-X. Xu, Dalton Trans. 22 (2001) 3352;
(b) M. Soler, P. Artus, K. Folting, J.C. Huffman, D.N. Hendrickson, G. Christou, Inorg. Chem. 40 (2001) 4902.

[9] N.E. Chakov, S.-C. Lee, A.G. Harter, P.L. Kuhns, A.P. Reyes, S.O. Hill, N.S. Dalal, W. Wernsdorfer, K.A. Abboud, G. Christou, J. Am. Chem. Soc. 128 (2006) 6975.

[10] A.G. Harter, N.E. Chakov, B. Roberts, R. Achey, A. Reyes, P. Kuhns, G. Christou, N.S. Dalal, Inorg. Chem. 44 (2005) 2122.

[11] S. Hill, N. Anderson, A. Wilson, S. Takahashi, N.E. Chakov, M. Murugesu, J.M. North, N.S. Dalal, G. Christou, J. Appl. Phys. 97 (2005) 10M510.

[12] R.M. Achey, P.L. Kuhns, A.P. Reyes, W.G. Moulton, N.S. Dalal, Phys. Rev. B 64 (2001) 064420.

[13] R.M. Achey, P.L. Kuhns, A.P. Reyes, W.G. Moulton, N.S. Dalal, Solid State Commun. 121 (2002) 107.

[14] T. Kubo, T. Goto, T. Koshiba, K. Takeda, K. Awaga, Phys. Rev. B 65 (2002) 224425.

[15] A.G. Harter, N.E. Chakov, R. Achey, A. Reyes, P. Kuhns, G. Christou, N.S. Dalal, Polyhedron 24 (2005) 2346.

[16] A. Morello, O.N. Bakharev, H.B. Brom, R. Sessoli, L.J. de Jongh, Phys. Rev. Lett. 93 (2004) 197202.

[17] W. Wernsdorfer, R. Sessoli, D. Gatteschi, Europhys. Lett. 47 (1999) 254.